Intermolecular Coulombic Decay of Molecular Clusters: Identification of the Decay Mechanism Using a New Hole-Population Analysis

J. Zobeley* and L. S. Cederbaum

Theoretische Chemie, Universität Heidelberg, Im Neuenheimer Feld 229, D-69120 Heidelberg, Germany

F. Tarantelli

Dipartimento di Chimica and Centro CNR C.I.S.M., Università di Perugia, I-06123 Perugia, Italy

Received: July 29, 1999; In Final Form: October 14, 1999

Singly ionized states of molecular clusters with an inner-valence vacancy have recently been shown to undergo an efficient electronic decay. The mechanism of the decay, which is absent in the isolated molecules that build up the clusters, is proposed to be of intermolecular Coulombic nature. As explicit example to further investigate this new decay process, the valence ionization spectrum of the $HF(H_2O)_2$ cluster is computed with the ADC(3) one-particle Green's function method. In the inner-valence part of the spectrum, characteristic dense line bundles due to the ultrafast electronic decay of the corresponding cationic states are observed. A new hole-population analysis method for the very many computed cationic states is presented. This method allows for a quantitative measure and characterization of the hole localization pattern of the cationic states. The dense line bundles which mimic the continuous decay distributions in our finite basis set approach are analyzed in detail. The resulting intermolecular character of the states confirms the recently proposed intermolecular Coulombic mechanism for the electronic decay in molecular clusters. The decay leads to dicationic states with two vacancies located on neighboring monomer units.

1. Introduction

The study of the electronic structure of clusters is a central subject of interest in chemical as well as in physical research for many years. A large and rapidly increasing number of experimental and theoretical studies on all kind of clusters emphasizes the importance of clusters, ranging from a better understanding of the fundamental properties of matter in general to practical applications in material science.[1,2] Although clusters often exhibit quite unique properties, their role in linking together the properties of the constituent isolated monomer units and the corresponding bulk material can hardly be overestimated. An especially active subfield in cluster science is the study of van der Waals clusters which includes such different species such as atomic rare gas clusters and hydrogen bonded molecular clusters.[3−5] These weakly bound systems are of particular interest in the exploration of intermolecular interactions.

In contrast to the multitude of studies on the electronic structure of the neutral ground state of clusters, there have been comparatively few studies on highly excited electronic states like singly ionized states of clusters, especially when considering weakly bound systems. This situation has started to change quite rapidly in the past few years (see, e.g., refs 6−9), not least because of the development of new experimental techniques and improved quantum-chemical methods of calculation on much faster computers.

An important and widespread method to produce singly ionized states in general is the photoionization of the corresponding neutral systems. Photoelectron spectroscopy is for a long time known as a powerful and specific method for the study of the electronic structure of molecular systems.[10,11] But nearly all experiments involving singly ionized states focus on either the energy region of outer-valence ionization (UV photoelectron spectroscopy (UV−PES)) or the energy region of core-ionization (X-ray photoelectron spectroscopy (XPS)).[7−9] The intermediate energy range of inner-valence ionization has encountered much less attention (see, e.g., refs 12−14). One important reason for this deficit, the lack of suitable radiation sources, has been removed during the last years by developing sufficiently monochromatized sources of radiation, with high enough intensity, that are tunable in the relevant energy range, of which the most prominent exponent is synchrotron radiation. The combination of monochromatized tunable synchrotron radiation with modern coincidence-detection techniques having the capability of simultaneous detection of photons, photoelectrons, and ionic (fragmentation) products in a cluster beam apparatus have made high spectral resolution experiments on free gas-phase clusters possible, at least in principle, in a wide energy range.

Excited states have finite lifetimes. Therefore, the study of the decay processes (lifetime, decay mechanism) of the singly ionized cationic states is of extremely high relevance for the understanding of the physical properties of the systems under investigation. In principle, excited electronic states can decay radiatively by photon emission and/or nonradiatively by electron emission (electronic decay). The preferred decay mechanism is highly dependent on the energy range of the excitation. For most systems it is well-known that energetically low-lying states, such as outer-valence ionized states, can only decay radiatively, while energetically high-lying states, like inner-shell ionized states, decay more efficiently by electronic decay.[15] A prominent representative of the latter is the Auger decay of core vacancies.[16] Very characteristic of the complementary decay processes

* Corresponding author. E-mail: c86@ix.urz.uni-heidelberg.de.

10.1021/jp992677i CCC: $18.00
Published on Web 12/01/1999

are the different lifetimes of the excited states in dependence of the energy region of excitation. States which can decay only radiatively (excited outer-shell vacancies) have long lifetimes compared to states which decay electronically (excited inner-shell vacancies). Also the sensitivity of the decay to the chemical environment strongly depends on the energy region of the excited state. While the radiative decay of outer-shell vacancies is very sensitive to the chemical environment, the electronic decay of inner-shell vacancies (Auger decay) is only weakly influenced (intra-atomic process).

The situation is much more complex in the intermediate energy region of inner-valence vacancies. Here, even the principal mechanism of the decay can be changed by the influence of the chemical environment. In typical small molecules the electronic decay of a single inner-valence vacancy (e.g., ionization of 2s orbitals in first-row atoms such as O, F, Ne) leading to a doubly ionized final state is not possible because of energetic reasons. The lowest lying doubly ionized states (two outer-valence vacancies) lie significantly higher in energy than the single inner-valence vacancies, mainly because of the strong Coulomb repulsion of the two holes in the dicationic states. As a consequence, the singly ionized inner-valence states of the molecules can decay only radiatively. The situation can change drastically as soon as the above-mentioned molecular unit interacts with a suitable chemical environment, e.g., in weakly bound molecular clusters. We have shown recently,[17,18] using large scale ab initio Green's function calculations, that excited electronic states of molecular clusters such as $(HF)_n$ or $(H_2O)_n$ ($n = 2-4$) with at least one inner-valence vacancy can efficiently decay electronically. The estimated lifetimes of the order of few femtoseconds are comparable to those typical for core vacancies. Very recently, these estimates have been nicely confirmed in a quantitative study on selected inner-valence F(2s) vacancies of the $(HF)_2$ system using configuration interaction methods with complex absorbing potentials (CAPs) to take into consideration the outgoing continuum electron.[19]

The principal mechanism of the decay of the inner-valence vacancies in molecular clusters, which has been proposed to be of intermolecular Coulombic nature, is presented in Figure 1 together with the relative energies of the involved electronic states. Figure 1a shows that whereas the ionization potentials (IPs) of the inner-valence vacancies in the molecular clusters are only slightly lowered compared to the isolated monomer molecules, the energy onset of doubly ionized states in the clusters is lowered drastically because of the appearance of a new kind of dicationic states with the two vacancies localized on different monomer units (two-site states). The reduced Coulombic interaction of the holes in the two-site states, because of their spatial separation, is responsible for the distinct energetic lowering compared to the states with both holes being localized on the same unit (one-site states) and leads to the opening of electronic decay channels for the inner-valence vacancies. Discovering the energetic availability of two-site dicationic decay channels, and observing unmistakable signs of efficient electronic decay of the inner-valence vacancies in the computed ionization spectra, prompted us to propose an intermolecular Coulombic decay (ICD) mechanism[17,18] for the inner-valence vacancies which is summarized schematically in Figure 1b. An outer valence electron at the monomer unit with the initial inner-valence vacancy drops into this vacancy and the resulting excess energy is used to eject an electron from the outer-valence of a neighboring unit. In clusters there is a large number of available decay channels of this type. In addition, the Coulomb matrix elements governing the decay rates are of nonnegligible

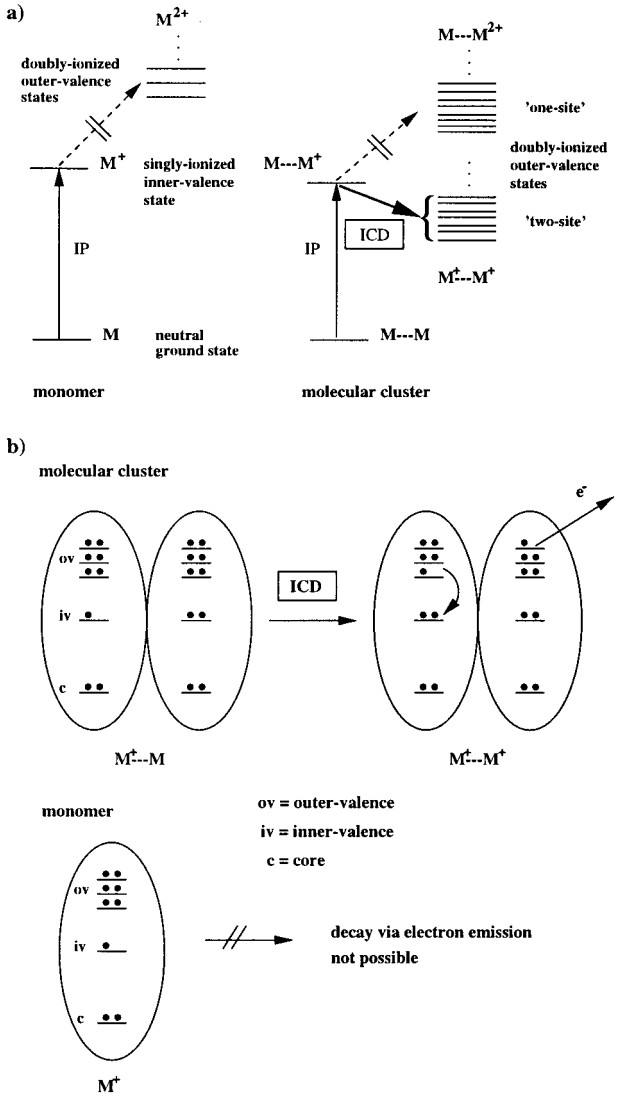

Figure 1. Schematic representation of the intermolecular Coulombic decay (ICD) of molecular clusters. (a) State diagram showing the energetic situation typical for a single inner-valence vacancy in the molecular cluster. In contrast to the isolated molecules, the inner-valence vacancy in the molecular cluster can efficiently decay electronically because of the accessible dicationic decay channels with the two vacancies localized on neighboring molecular units. (b) ICD mechanism represented by the changes in the electronic configurations of the involved neighboring molecules.

magnitude at the relatively small kinetic energies of the outgoing electron involved. These facts make up for an efficient and fast energy transfer mechanism between the units constituting the cluster.

Up to now the intermolecular character of the decay process has mainly been deduced by inspection of the physical nature of the energy-permitted dicationic decay channels. In the present paper we investigate the ICD mechanism of inner-valence vacancies of molecular clusters in direct fashion. For this purpose, an exemplary study of the singly ionized states of the cyclic $HF(H_2O)_2$ cluster has been carried out. The cationic states of the cluster result from large scale ab initio Green's function calculations on the ionization spectrum of the neutral ground state system. The resulting cationic state distributions are then analyzed in detail with a new hole-population analysis. This method allows us to characterize and classify the very many calculated cationic states according to their spatial hole-density distribution in a quantitative way. This is especially important

in the inner-valence region, with its characteristic large number and high density of states due to strong correlation and electronic decay effects. In our finite basis set calculations, the energy broadening due to decay of an ionized state appears as a dense cluster of states with low spectral intensity (satellite states) centered around the decaying state.[18] This characteristic satellite structure, which mimics a continuous intensity distribution, describes the coupling of the decaying cationic state to the energetically accessible double ionization continuum. The detailed analysis of the hole-density in these dense line distributions, therefore, provides direct insight into the physical nature of the decay process and can unambiguously confirm the proposed intermolecular mechanism.

The paper is organized in the following way. In section II we briefly describe the methods used to calculate the valence singly ionized states of the cluster as well as their available decay channels via electron ejection. section III then introduces the hole-population analysis for the characterization of the very many calculated cationic states. In section IV the results on the ICD of the singly ionized inner-valence vacancies of the HF-$(H_2O)_2$ cluster are presented and discussed. Finally, section V gives a summary of the essential points as well as an outlook on possible experiments and extensions of the theoretical studies. In the Appendix the spin-free working equations of the hole-population analysis are listed for completeness.

2. Methods and Computational Details

The valence ionization spectra of the $HF(H_2O)_2$ cluster and the isolated corresponding molecules HF and H_2O have been computed using the third-order algebraic diagrammatic construction scheme (ADC(3)) for the approximate evaluation of the poles and residues of the one-particle Green's function.[20] The ADC scheme in general, as well as the ADC(3) scheme in particular, which is also known as the extended two-particle-hole Tamm−Dancoff approximation (2ph-TDA), have been discussed in detail in the literature.[20−23] We therefore only summarize some of the important properties of the method. The ADC(n) scheme for a given order n of many-body perturbation theory transforms the evaluation of the Green's function or propagator to a Hermitian eigenvalue problem of the corresponding ADC matrix. In the specific numerical approach used in this work (ADC(3)/1p-GF program package[24,25]) instead of evaluating the one-particle Green's function directly, the so-called self-energy, which is related to the one-particle Green's function via the Dyson equation (see, e.g., refs 26 and 27), is evaluated with the ADC scheme. The resulting ADC(3) matrix has a characteristic block structure. A small one-particle block built up from one-hole (1h) and one-particle (1p) configuration contributions is coupled to a large ionization block built up from two-hole-one-particle (2h1p) configuration contributions, and an even larger affinity block built up from two-particle-one-hole (2p1h) configuration contributions, the latter block mainly determining the dimension of the ADC matrix. All configuration classes are labeled with respect to the Hartree−Fock configuration of the neutral ground state. The eigenvalues of the ADC matrix are the ionization potentials and electron affinities of the system, while the spectroscopic factors of the corresponding transitions are directly related to the eigenvectors. With the ADC(3) scheme cationic states perturbatively derived mainly from 1h configurations (main states) are described consistently through third order perturbation theory, whereas cationic states perturbatively derived mainly from 2h1p configurations (satellite states) are described through first-order perturbation theory. All computed quantities are size-consistent in any order of perturbation theory.

To extract many eigensolutions of this large-scale eigenvalue problem with dimensions typically of the order of 10^4-10^5, subspace iteration methods have to be used. Preliminarly, an approximation procedure has proved to be successful in many applications (see, e.g., refs 18, 25, and 28). Because we are only interested in the cationic solutions of the eigenvalue problem, it is convenient to replace the energetically well-separated large affinity block of the ADC matrix with a lower dimensional block in a first step. This smaller block is calculated by projecting the anionic matrix onto a low-lying subspace via a relatively small number of block-Lanczos iterations, so that the lowest moments of the spectral distribution of affinity poles is preserved.[29] The projected band matrix is then diagonalized and the coupling to the rest of the configuration space transformed accordingly.

Although the configuration spaces of the ADC eigenvalue problems are much smaller compared to similar configuration interaction calculations, the adequate description of the cationic states of extended systems, such as molecular clusters leads, even after prediagonalization/reduction of the affinity block, to large-scale eigenvalue problems with dimensions still of the order of 10^3-10^4 and dense-lying eigensolutions in the inner-valence region of the spectra. Therefore, in many cases full diagonalization of the reduced ADC matrixes is no longer possible. In these cases, again the moment-preserving block-Lanczos diagonalization procedure has been shown in numerous applications to be ideally suited for the approximate solution of the eigenvalue problems.[17,18,28] The method provides a convergence rate on the spectral envelope of the main space components (1h/1p) which is exponential in the number of iterations and the line widths.[29] Because of the correct description of the spectral envelope, the regions with dense-lying roots are described correctly already after relatively few iterations, even though the states may not be fully converged individually. It should be noted here that the spectral envelope around a dense state distribution is generally the only physically meaningful property to describe the corresponding spectra. In the case that the dense state distribution mimics a nonstationary wave packet, due to the discrete finite basis set approach, the spectral envelope is in fact the only properly defined quantity.

The very many calculated cationic states, especially in the inner-valence region of the ionization spectra, have been further characterized according to the spatial distribution of the one-hole density of the ADC eigenvectors, using a new hole-population analysis. This analysis allows to gain deeper insight into the physical nature of the cationic states, as well as providing a classification scheme for the many states. We shall describe it in detail, especially with respect to its importance in the analysis of the electronic decay of the inner-valence cationic states, in section III.

To evaluate possible electronic decay channels for the inner-valence cationic states, we have calculated the outer-valence dicationic states of the systems with the direct second-order ADC(2) scheme for the evaluation of the particle−particle propagator.[30−32] Here, the configuration space of the ADC matrix comprises all dicationic two-hole (2h) and three-hole-one-particle (3h1p) configurations with respect to the neutral Hartree−Fock ground state. Dicationic states which are perturbatively derived mainly from 2h configurations (main states) are calculated consistently through second-order perturbation theory whereas dicationic states perturbatively derived from 3h1p configurations (satellite states) are calculated consistently through first-order perturbation theory. For the approximate

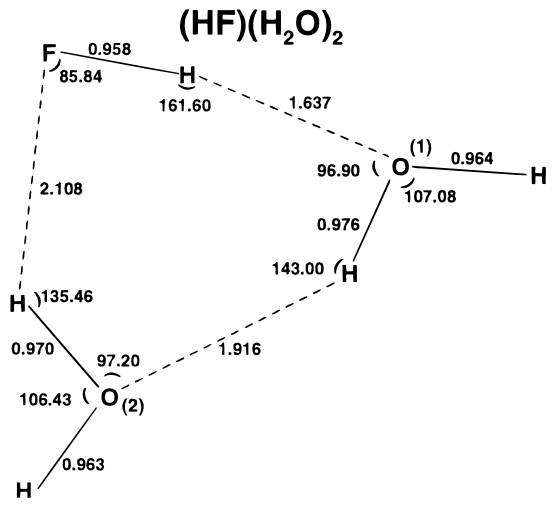

Figure 2. Neutral ground-state structure of the cyclic $HF(H_2O)_2$ cluster used in the calculation of the ionization spectrum. The nonplanar C_1-symmetric structure taken from ab initio literature data has been slightly modified into the shown planar-C_s symmetric structure in order to facilitate the large-scale Green's function calculations (Nuclear distances are given in angstrom, angles in degree).

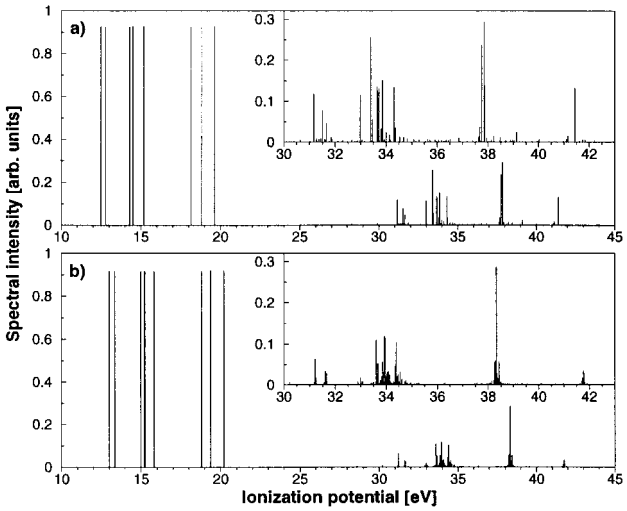

Figure 3. Basis set dependence of the computed valence ionization spectrum of the $HF(H_2O)_2$ cluster. (a) cc-pVDZ basis set, (b) aug-cc-pVDZ basis set. The vertical bars indicate the individual computed transitions of height proportional to their pole strength. The inner-valence region (≈30−45 eV) of the calculated spectra is shown on an expanded energy scale. Besides a slight shift of the whole spectrum the largest effect of augmenting the cc-pVDZ basis set with a set of diffuse s,p,d functions is the enhanced density of states in the line bundles representing the electronic decay of the inner-valence vacancies.

solution of the resulting large-scale ADC eigenvalue problem of the dicationic states the block-Lanczos procedure[29] has been used.

The calculated outer-valence dicationic states in the energy region accessible via decay of inner-valence cationic states have been further characterized according to the spatial distribution of the two-hole density with respect to the 2h configuration space (main space) using a two-hole population analysis.[33] With this analysis one decomposes the 2h contributions to the ADC eigenvectors into their localized atomic components. The terms describing the localization of the two holes on a single atomic center make up the one-site contributions; the terms describing the localization of the two holes on pairs of atomic sites, with each of them carrying one hole, define the two-site contributions.

All Green's function calculations of the singly and doubly ionized states have been performed at the ab initio equilibrium geometries of the neutral ground-state systems.[34] To facilitate the calculations, however, a slightly modified planar C_s -symmetric model structure has been used for the $HF(H_2O)_2$ cluster instead of the nonsymmetric C_1-structure taken from the literature. The structure of the C_s -symmetric $HF(H_2O)_2$ system is shown in Figure 2. The planar model structure has been obtained by simply rotating the monomer units relative to each other in a way that the intramolecular parameters are not changed at all, and the intermolecular parameters are changed as little as possible. The higher symmetry of the model structure leads to a decoupling of the eigenvalue problem into lower dimensional problems for each irreducible representation. This permits the use of larger basis sets and active configuration spaces, leading to a more accurate description of the electronic decay effects under investigation. The results of Green's function calculations with relatively small standard Gaussian basis sets have been carefully compared for both the C_1- and C_s-symmetric structure showing that the results are virtually unaffected.

The orbital energies and Coulomb-integrals resulting from Hartree−Fock calculations on the neutral ground state with the GAMESS−UK program package[35] serve as input for the corresponding ADC calculations. As basis set for all calculations presented here the correlation-consistent Dunning basis set of double-ζ quality including polarization functions and augmented by a set of diffuse s, p, and d-functions on each of the atomic centers (aug-cc-pVDZ[36]) has been used. This basis set has proved to be a good compromise between feasibility and accuracy of the calculation, especially with respect to the reliability of the description of the decay phenomena, in the calculation of similar molecular clusters such as the small $(HF)_n$ and $(H_2O)_n$ clusters.[17,18] Here, we only want to illustrate the importance of diffuse functions for the qualitatively correct description of the decay distributions in the calculated spectra. This is done by comparing the calculated ionization spectra of the $HF(H_2O)_2$ cluster obtained with the cc-pVDZ and the aug-cc-pVDZ basis set in Figure 3. It can be clearly seen that, although the outer-valence part (≈12−21 eV) of the spectrum is only shifted toward higher energies when augmenting the cc-pVDZ basis set with a set of diffuse functions, the inner-valence part (≈30−45 eV) is changed substantially in its character. The most eye-catching effect when augmenting the basis set with diffuse functions is the drastically enhanced density of states in the line bundles which are the discrete basis representation of continuous intensity distributions. In some cases only a single line is observed with the cc-pVDZ basis set instead of a line bundle with the aug-cc-pVDZ basis set (see, e.g., the change in the spectrum at ≈41−42 eV) meaning that the cc-pVDZ basis set cannot describe the decay effects correctly. It has been shown in a previous study on small $(HF)_n$ clusters[18] that further augmenting the aug-cc-pVDZ basis set or using higher quality standard basis sets augmented by diffuse functions does not change the description of the decay in a qualitative way.

In all calculations the 1s-core orbitals of the fluorine and oxygen atoms have been excluded from the active configuration space as well as their highest lying virtual counterparts. A further restriction of the active configuration space has been enforced in a separate set of calculations to carry out the hole-population analysis. As input of the hole-population analysis the full 1h and 2h1p contributions of the ADC(3) eigenvectors are needed (see section III). On the other hand, the computational effectiveness of the block-Lanczos procedure is essentially lost when used to compute many complete and accurate eigenvectors

instead of the rapidly converging distribution of main space components. Similarly, other preconditioned iterative diagonalization techniques tend to converge extremely slowly, if at all, on the dense line bundles describing the cluster decaying hole states. To quickly get around this problem, we have restricted the size of the configuration spaces (through virtual orbital selection) until full diagonalization with standard methods was possible. The influence of the restriction on the resulting spectra has been carefully investigated. These results are presented in section IV D when discussing the hole-population analysis of the cationic states of the $HF(H_2O)_2$ cluster.

3. Characterization of the Cationic States: Hole-Population Analysis

A very characteristic property of the valence ionization spectra for even relatively small molecular systems is the large number and high density of cationic states in the inner-valence region. This general situation is even more pronounced in extended systems like molecular clusters. The strong coupling of nearly degenerate cationic configurations, in combination with hole localization effects, results in distinct correlation effects which lead to a redistribution of configuration contributions over some or even many cationic states. This effect is well-known as the breakdown of the independent particle picture of ionization.[37] Any one of the very large number of states resulting from this strong interaction gains only small spectral intensity in the ionization spectrum (satellite states) because of their small 1h configuration components, but collectively these states may produce quite distinct spectral profiles in the inner-valence region, owing to their number and high density. Because of the lack of an appropriate analysis, only very little is known about the physical nature of the many satellite states up to now.

As we have shown recently,[17,18] the electronic decay of inner-valence vacancies is mimicked in the calculated ionization spectra by dense line bundles of satellite states that group around the decaying states, because of the finite discrete basis set description. To analyze these dense state distributions in detail we have set up a hole-population analysis for the cationic states. This hole-population analysis, which decomposes the hole-density of the cationic states into its localized atomic contributions, permits the characterization and classification of the states based on the localization pattern of their electron vacancy. This concise information is particularly precious in regions of high density of states such as the ones we are investigating.

The outer-valence cationic states are typically derived from 1h configurations (main states), and therefore the hole-density analysis of their 1h components is sufficient for characterization. For the inner-valence satellite states, which are mainly derived from 2h1p configurations, a meaningful hole-density analysis has to include the 2h1p configuration space too.

The basic equation for the density (Δr) of an electron vacancy (hole-density) at space position r, in the n-th cationic state Ψ_n^{N-1} resulting from sudden removal of an electron from the neutral ground-state Ψ_0^N of the system, reads

$$\Delta(r) = -\langle \Psi_n^{N-1} | \hat{\rho}(r) | \Psi_n^{N-1} \rangle + \langle \Psi_0^N | \hat{\rho}(r) | \Psi_0^N \rangle \qquad (1)$$

Here, $\hat{\rho}(r)$ is the usual density operator in Heisenberg representation, which is related to the basic field operator $\hat{\psi}(r)$ through the expression $\hat{\rho}(r) = \hat{\psi}^\dagger(r)\hat{\psi}(r)$. Expansion of the field operator in the set of molecular one-particle functions $\{\phi_p\}$ (Hartree−Fock orbitals) of the neutral system as

$$\hat{\psi}(r) = \sum_p \phi_p(r) a_p \qquad (2)$$

results in the following expression of the hole-density $\Delta(r)$:

$$\Delta(r) = \sum_{p,q} \phi_p^*(r)\phi_q(r) \underbrace{[-\langle \Psi_n^{N-1} | a_p^\dagger a_q | \Psi_n^{N-1} \rangle + \langle \Psi_0^N | a_p^\dagger a_q | \Psi_0^N \rangle]}_{\Delta_{pq}} \qquad (3)$$

where a_i ($a_i^\dagger$) denotes a destruction (creation) operator for an electron in orbital ϕ_i. We now approximate the exact neutral ground-state $|\Psi_0^N\rangle$ to be uncorrelated (Hartree−Fock)

$$|\Psi_0^N\rangle = |\Phi_0\rangle \qquad (4)$$

and expand the exact cationic state $|\Psi_n^{N-1}\rangle$ in terms of configuration classes with respect to the neutral Hartree−Fock ground-state configuration:

$$|\Psi_n^{N-1}\rangle = \sum_i x_i \underbrace{a_i|\Phi_0\rangle}_{\text{1h config}} + \sum_{r,i>j} x_{rij} \underbrace{a_r^\dagger a_i a_j |\Phi_0\rangle}_{\text{2h1p config}} + ... \qquad (5)$$

Here and in the following, indices $i,j,k,...$ label the occupied orbitals and $r,s,t,...$ the virtual orbitals of the Hartree−Fock neutral ground state.

The ADC(3) scheme used to calculate the cationic states includes the cationic 1h and 2h1p configuration classes. Therefore, the analysis of the charge density of the cationic states calculated with the ADC(3) scheme takes into consideration only the first and second term in eq 5 [(1h+2h1p) hole-density]. Consideration of the first sum only leads to a hole-density in the 1h configuration space (1h hole-density). In the following the equations are derived for the full (1h+2h1p) hole-density. The formulas for the 1h hole-density can be obtained easily by omitting all 2h1p contributions.

After insertion of eq 5, truncated to the first two terms, into eq 3, the hole-density matrix elements Δ_{pq} read

$$\begin{aligned}\Delta_{pq} = &-\sum_{i,j} x_i^* x_j \langle \Phi_0 | a_i^\dagger\, a_p^\dagger a_q a_j | \Phi_0 \rangle \\ &-\Big(\sum_{r,k,i>j} x_{rij}^* x_k \langle \Phi_0 | a_j^\dagger\, a_i^\dagger a_r a_p^\dagger a_q a_k | \Phi_0 \rangle\Big) - (p \leftrightarrow q)^* \\ &-\sum_{\substack{r,i>j \\ s,k>l}} x_{rij}^* x_{skl} \langle \Phi_0 | a_j^\dagger\, a_i^\dagger a_r a_p^\dagger a_q a_s^\dagger a_k a_l | \Phi_0 \rangle \\ &+\langle \Phi_0 | a_p^\dagger a_q | \Phi_0 \rangle \end{aligned} \qquad (6)$$

Evaluation of the above matrix elements finally yields the following equations for the (1h+ 2h1p) hole-density matrix elements:

$$\begin{aligned}\Delta_{ij} &= x_j^* x_i + \sum_{r,k} x_{r[jk]}^* x_{r[ik]} \\ \Delta_{ri} &= -\sum_j x_{r[ij]}^* x_j \\ \Delta_{rs} &= -\sum_{i>j} x_{rij}^* x_{sij}\end{aligned} \qquad (7)$$

where we have defined

$$x_{r[ij]} = \begin{cases} x_{rij} & \text{for } i > j \\ 0 & \text{for } i = j \\ -x_{rji} & \text{for } i < j \end{cases} \tag{8}$$

Spin-symmetrization of the hole-density matrix elements in the $M_s = {}^1/_2$ space leads to the spinless doublet hole density which is used in the implementation of the hole-population analysis. The spin-free equations for the hole-density matrix elements are given in the Appendix.

For the spatial hole-population analysis of the cationic states, the hole-density eq 3 is rewritten in terms of the localized atomic orbital basis functions $\{\chi_\mu\}$:

$$\begin{aligned} \Delta &= \sum_{p,q} \Delta_{pq} \phi_p^* \phi_q \\ &= \sum_{p,q} \Delta_{pq} \sum_{\mu\nu} c_{\mu p}^* c_{\nu q} \chi_\mu^* \chi_\nu \end{aligned} \tag{9}$$

Regrouping of the basis functions χ_μ according, e.g., to their atomic origins *A*, *B*, ..., in a Mulliken-like manner results in

$$\Delta = \sum_{A,B} \sum_{p,q} \Delta_{pq} \sum_{\substack{\mu \in A \\ \nu \in B}} c_{\mu p}^* c_{\nu q} \chi_\mu^* \chi_\nu \tag{10}$$

The integral of this expression

$$1 = \sum_{A,B} Q_{AB} \tag{11}$$

defines a partitioning of the electron vacancy represented by the *hole-population matrix* **Q** with matrix elements

$$Q_{AB} = \sum_{p,q} \Delta_{pq} \sum_{\substack{\mu \in A \\ \nu \in B}} c_{\mu p}^* S_{\mu\nu} c_{\nu q} \tag{12}$$

where $S_{\mu\nu}$ are the overlap matrix elements between atomic basis functions χ_μ and χ_ν.

Equation 12, together with the spin-free counterpart of eq 7, now provides a well-defined and quantitative way to analyze the spatial hole distribution of the very many calculated cationic states in terms of their atomic contributions. In cases where the influence of different groups of basis functions, e.g., nondiffuse and diffuse ones, on the hole-density is of interest, the basis functions can be split further into several subgroups A_1, ...A_n, B_1, ...B_n on the atomic centers *A*,*B*.

4. Intermolecular Coulombic Decay (ICD) of Singly Ionized Inner-valence States of the $HF(H_2O)_2$ Cluster

A. The $HF(H_2O)_2$ Cluster. The small mixed H_2O/HF clusters have acquired substantial scientific interest, not least because of their prototype character in the study of hydrogen-bonding between nonequivalent monomer units.[34,38,39] IR-spectroscopical studies[40] on mixtures of H_2O/HF in Ar-matrix have resulted in the unambiguous detection of several species such as the two possible open-chain dimers of $(H_2O)HF$ and the $H_2O(HF)_2$ trimer. The existence of the $HF(H_2O)_2$ trimer has been strongly assumed but not yet proved unambiguously in the experiments.

Ab initio studies[34] on the neutral ground-state structure of $HF(H_2O)_2$ have resulted in a single cyclic minimum structure with C_1-symmetry. In this structure each of the monomer units acts simultaneously as H-donor and H-acceptor in the hydrogen bonds. The two H_2O units are nonequivalent with one of them acting as H-donor in the hydrogen bond with the HF unit, the other acting as H-acceptor (see Figure 2).

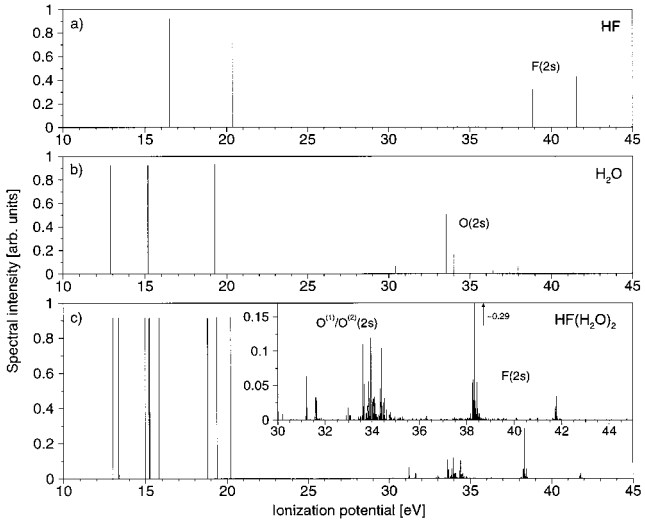

Figure 4. Valence ionization spectrum of the $HF(H_2O)_2$ cluster in comparison with the spectra of the isolated molecules HF and H_2O calculated with the ADC(3)/1p-GF method. The vertical bars indicate the individual computed transitions of height proportional to their pole strength. The inner-valence part (≈30−45 eV) of the calculated cluster spectrum is also shown on an expanded energy scale. In contrast to the isolated molecules, dense line bundles due to the electronic decay of the singly ionized inner-valence F(2s) and O(2s) vacancies are clearly visible. These line bundles mimic continuous intensity distributions in the discrete finite Gaussian basis set representation (aug-cc-pVDZ).

We have chosen the cyclic $HF(H_2O)_2$ cluster for our exemplary study of the ICD of singly ionized inner-valence vacancies for several reasons. One reason is that the size and structure of the system, with each monomer unit having two hydrogen-bonded neighboring units, make it an ideal candidate to show very distinct signs of electronic decay even in moderate-size discrete Gaussian basis set calculations. In addition, the nonequivalence of the molecular units in the mixed trimer cluster enhances the amount of information that can be extracted from the study of the decay mechanism and its determining factors, compared to a cluster of equivalent units, such as, e.g., $(HF)_3$. Therefore, the system is on one hand complex enough to allow us to demonstrate the diagnostic value of the computational and analytical tools developed, but it is on the other hand small enough to be treated with acceptable accuracy in reasonable time.

B. The Ionization Spectrum of the $HF(H_2O)_2$ Cluster: Signs of an Efficient Electronic Decay. The calculated valence ionization spectrum of the $HF(H_2O)_2$ cluster is compared to the known ionization spectra of the corresponding isolated molecules H_2O[41,42] and HF[43,44] in Figure 4. Because of the weakly bound character of the system, the valence ionization spectrum of $HF(H_2O)_2$ can be analyzed in terms of contributions from the interacting molecules H_2O and HF. Therefore, the ionization spectra of the isolated H_2O and HF molecules should be briefly discussed as reference first. All spectra presented in Figure 4 are separated into two distinct regions by an energy gap of ≈15 eV. The outer valence region in HF (≈15−21 eV) consists of two main peaks which result from ionization out of the 1π and 3σ orbitals with essentially F(2p) character, respectively. Each state is related with the ionization of a specific orbital, indicating the validity of the independent particle picture of ionization in this energy region. The situation is similar in the outer-valence of the ionization spectrum of the H_2O molecule (≈12−20 eV). Here, because of the C_{2v}-symmetry, three main peaks are

observed which result from ionization of the $1b_1$, $3a_1$, and $1b_2$ orbitals, with essentially O(2p) character, respectively.

In the inner valence region of the two spectra, the situation is different. In the HF spectrum, instead of observing a single peak resulting from ionization out of the 2σ orbital with mainly F(2s) character (as expected in the independent particle picture), the spectral intensity is distributed mainly over two peaks with comparable intensity. This observed line splitting is due to a partial breakdown of the independent particle picture of ionization[37] and is typical for the inner valence region of many molecular systems. The breakdown effect can be understood in terms of strong configuration interaction between quasi-degenerate inner-valence single-hole (1h) configurations and higher excited configurations, such as two-hole-one-particle (2h1p) configurations, involving the additional excitation of an outer-valence electron. These interactions then lead to a redistribution of the 1h configuration contributions to the spectral intensity over several or even many peaks in the spectrum and destroy the simple picture of main lines corresponding to 1h configurations, sometimes accompanied by a series of satellite lines corresponding to 2h1p configurations following at higher energies.

This breakdown effect is even more enhanced in the inner valence region of the H_2O molecule ($\approx$30−40 eV). Here, instead of one main line due to ionization out of the $2a_1$ orbital with mainly O(2s) character, the spectral intensity is distributed over several lines in an energy range of about 8 eV with at least four lines having major contributions. This enhanced, compared to HF, breakdown effect is at least partly due to the lower symmetry of the H_2O molecule leading to stronger interactions between inner-valence configurations.

It should be noted here that there exist many energy levels in the inner-valence region of the systems under discussion (e.g., Rydberg states) which are not visible in the calculated ionization spectra in Figure 4. This is due to the fact that spectral transitions to states derived mainly from excited configurations (e.g., 2h1p configurations with a diffuse Rydberg-like 1p contribution) gain only very small intensity in ionization spectra calculated or recorded in the framework of the sudden approximation (see, e.g., ref 37 and references therein) because of their negligible 1h contributions. Additionally, the basis set used in the calculations has not been optimized to represent this kind of states because they do not play a role in the present study.

We now turn to the valence ionization spectrum of $HF(H_2O)_2$, which should be analyzed in comparison with the isolated constituent units H_2O and HF. The outer-valence region ($\approx$11−20 eV) consists of nine main peaks. These peaks are due to ionization out of the nine outer-valence orbitals of $HF(H_2O)_2$ resulting from the intermolecular interaction among the orbitals of the constituent monomer units. These orbitals are linear combinations having contributions on the different units. The former degeneracy of the F(1π) has been removed because of the intermolecular interaction and symmetry lowering.

The situation in the inner-valence region ($\approx$30−45 eV) is much more complex. Here, a very rich structure of dense lying groups of lines are centered around lines with somewhat higher intensity. The positions of these dense distributions correspond quite closely to the peak positions in the isolated molecules. The two dense distributions between 36 and 42 eV, e.g., obviously correspond to the former two F(2s) peaks in the isolated HF molecule and gain their spectral intensity—as we will show in section IVD using the hole-population analysis—from 1h configuration contributions exclusively localized on HF. The more complex structure between 30 and 35 eV corresponds to overlapping and strongly mixing O(2s) peaks from the two nonequivalent H_2O monomer units in the cluster. The 1h configurations responsible for the spectral intensity of these peaks are linear combinations having contributions on both H_2O units. The character of the very many calculated satellite lines appearing in the inner-valence of the $HF(H_2O)_2$ spectrum will be discussed further in detail in section IVD using the hole-population analysis introduced in section III.

The main difference between the inner-valence region of the spectra of the monomers and the molecular cluster is that, in place of the distinct isolated lines of the monomer spectra, dense bundles of line fine structure appear in the spectrum of the cluster, centered about the former single lines. As we have shown recently in a study on the small $(HF)_n$ clusters,[17,18] these dense line bundles grouped around a state mimic, in a discrete basis set approach, the broadening of the spectral lines due to decay. The satellite states in these dense state distributions represent the coupling of the decaying cationic state to the continuum of accessible dicationic decay channels. Analyzing the possible dicationic decay channels resulted in the proposal of the ICD mechanism. To definitively prove the proposed mechanism and to gain deeper insight into its details, we analyze in the following the nature of the ionic states involved in the decay distributions, as well as the possible final dicationic states.

C. Evaluation of Possible Decay Channels. The possible dicationic states that can be reached via autoionization decay of the inner-valence hole states of the $HF(H_2O)_2$ cluster have been calculated with the ADC(2) scheme for the evaluation of the particle−particle propagator.[30,31] To emphasize the peculiarity of the situation in molecular clusters, the results are compared to those on the isolated molecules HF and H_2O, as shown in Figure 5.

The situation in the isolated HF and H_2O molecules is very simple: The inner-valence F(2s) or O(2s) singly ionized states are about 4 eV lower in energy than the lowest doubly ionized states. Therefore, simply because of energetic reasons, the decay of the inner-valence cationic states via electron emission is not possible (IP(inner valence) > DIP(outer valence)). The excited states can only decay radiatively. In agreement with this, as we have seen, no traces of electronic decay are found in the calculated ionization spectra of the molecules. In sharp contrast with this situation, strong signs of efficient electronic decay of the inner-valence vacancies can be found as soon as the monomer units interact with each other building a weakly bound molecular cluster like $HF(H_2O)_2$ (see Figure 4). As can be seen easily in this case, a large number of dicationic states is now accessible via electronic decay. Both the H_2O(2s) and the HF-(2s) inner-valence vacancies are embedded in a relatively dense distribution of dicationic states. The electronic decay should be possible on energetic reasons because some or even many outer-valence dicationic states are lower in energy than the singly ionized inner-valence states.

To understand this drastic change in behavior between isolated molecules and weakly bound cluster, it is important to analyze the character of the accessible dicationic decay channels in some detail. This has been done using a two-hole population analysis[33] that decomposes the two-hole density of the dicationic states into their localized atomic contributions, and thereby into components describing the two-hole distribution over the constituent units of the cluster. Because of the main state character of the dicationic states with both holes in the outer-valence, it is sufficient to consider the 2h configuration space contributions of the dicationic eigenvectors in the analysis only. The composition of the dicationic states of the cluster in terms

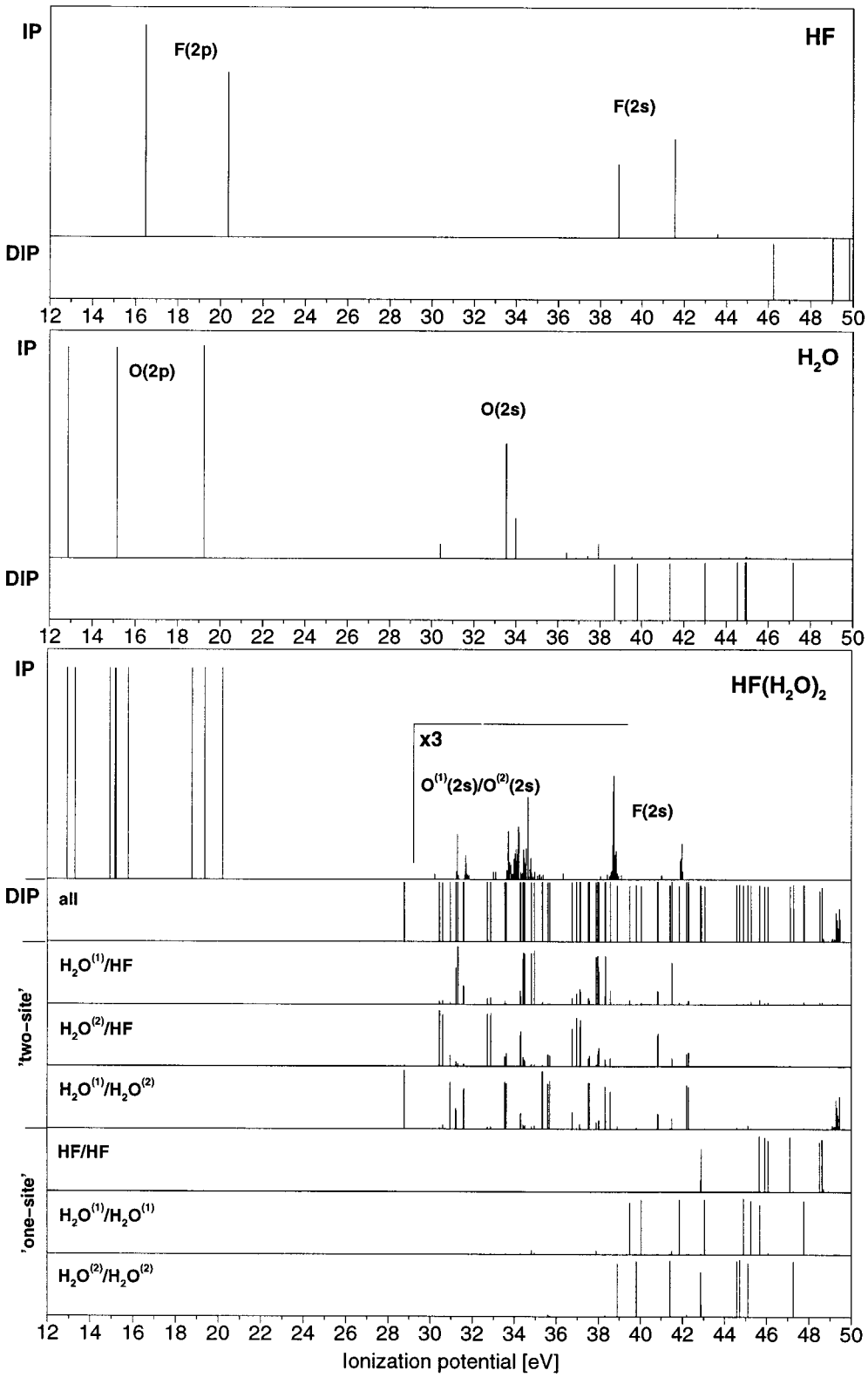

Figure 5. Evaluation of energy-permitted dicationic decay channels of the $HF(H_2O)_2$ cluster in comparison with the situation in the isolated molecules HF and H_2O. The vertical bars indicate the individual computed transition of height proportional to their pole strength. The DIPs corresponding to transitions to outer-valence dicationic states are shown below the respective IPs. The 2h-pole strength of the individual dicationic states of the $HF(H_2O)_2$ cluster is further decomposed into contributions describing the two-hole density on pairs of molecular units. The dicationic states can thus be classified in one-site and two-site states. Essentially only two-site states are accessible to the electronic decay of the inner-valence vacancies in the cluster.

of contributions from the different monomer units are shown in Figure 5. An evident observation is that the vacancies of the dicationic states are either localized both on the same unit (one-site states) or each on a different units (two-site states). The onset of the one-site states is much higher in energy (by $\approx$10 eV) than the onset of the two-site states (i.e., the double ionization threshold). An important fact is that, just like in the isolated molecules, the one-site dicationic states on a specific

cluster unit are higher in energy than the corresponding inner-valence cationic states on the same unit. Therefore, the dicationic HF one-site states are not accessible at all to the decay of any of the singly ionized states, and only very few dicationic H_2O one-site states are in principle energetically available for one-hole states localized on HF, but have negligible overlap with the latter because of the localization of the vacancies on different monomer units. Therefore, one can conclude that, like in the isolated monomers, one-site dicationic states are not available for electronic decay of inner-valence vacancies in the molecular cluster $HF(H_2O)_2$.

The situation is totally different for the two-site states, which of course do not exist for the isolated monomers. As already noted, the existence of these states lowers the double ionization threshold substantially, because of the largely reduced Coulomb interaction of the spatially separated hole-charges. The vast majority of these distributed states has the two holes localized on two neighboring monomer units, but there is also a nonnegligible number of states with hole-charge contributions on all three monomer units. This delocalization of the two holes on three monomer units can be understood in terms of dicationic configurations delocalized over the two H_2O units mixing with dicationic configurations with at least one hole on the HF unit. This large number of two- and even three-site states (because of the configuration mixing) is accessible for electronic decay of the inner-valence cationic states. When the latter are localized on a single cluster unit, as is the case for the F(2s) vacancies, we can therefore conclude that the electronic decay has to be intermolecular, leading to dicationic states having the two holes distributed over at least two neighboring units.

D. Hole-Population Analysis of the Decay Distributions of the Inner-Valence Cationic States. The very many calculated cationic states, especially in the inner-valence region of the ionization spectrum of the $HF(H_2O)_2$ cluster, have been characterized according to their spatial hole-charge distribution with the hole-population analysis introduced in section III. With this method the full 1h and 2h1p configuration components of the ADC(3) eigenvectors of the calculated cationic states are partitioned in contributions on the different atomic centers. As already mentioned in section II, to obtain accurate and complete eigenvectors by full diagonalization of the ADC matrixes, the latter have to be reduced in size by restricting the configuration space. This has been done by reducing the number of active one-particle functions (Hartree−Fock orbitals) so that only virtual orbitals with energy lower than a given threshold are taken into account. The calculated ionization spectra obtained with different sizes of the active configuration space for the aug-cc-pVDZ basis set are presented in Figure 6. It is clearly visible that, apart from a shift of the inner-valence part of the spectrum to higher energies when reducing the active configuration space, the line bundles themselves, and therefore the description of the decay, are only slightly affected. The widths of the bundles are broadened to some extent when restricting the size of the active configuration space because of the artificially enhanced breakdown effects which are due to reduced flexibility of the configuration space. It is clear, however, that the reduction of the ADC matrix by truncation of the configuration space within an appropriately chosen basis set preserves a very reliable description of the decay lines, in contrast to a size reduction obtained by restricting the Gaussian basis itself, e.g., by discarding the set of diffuse functions (see Figure 3). All results of the hole-population analysis presented in the following are based on the ADC(3) calculations with the restricted active configuration space in the aug-cc-pVDZ basis

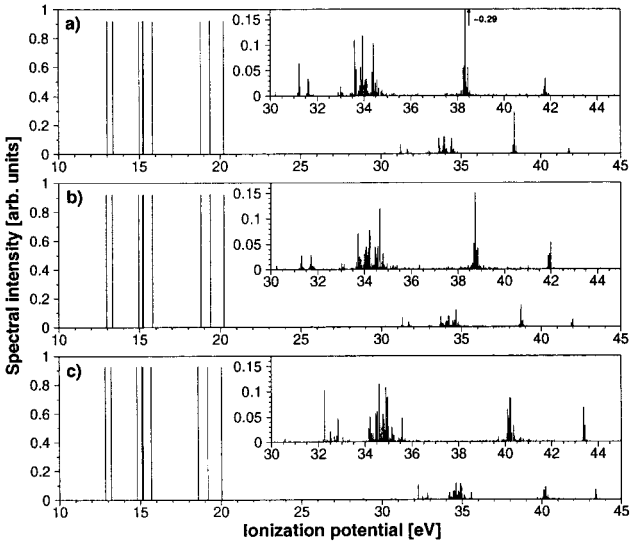

Figure 6. Dependence of the valence ionization spectrum of the $HF(H_2O)_2$ cluster on the size of the active configuration space used in the ADC(3)/1p-GF calculation with the aug-cc-pVDZ basis set. (a) full configuration space excluding only F(1s) and O(1s) core orbitals (114 active orbitals, block-Lanczos diagonalization), (b) restricted configuration space excluding orbitals with energies $\epsilon_i > 3.4$ au (96 active orbitals, block-Lanczos diagonalization), (c) restricted configuration space excluding orbitals with $\epsilon_i > 1.2$ au (58 active orbitals, full diagonalization).

set including orbitals with energies <1.2 au. The corresponding ionization spectrum is presented in Figure 6c. In this case the dimension of the ADC matrix after prediagonalization of the affinity block is of the order of 4800 for the larger A′ symmetry representation.

The results of the hole-population analysis are presented in Table 1. For reasons of simplicity only selected states, characteristic of the different spectral regions, are shown. They have been chosen to be fully representative of the very large number of remaining states in each of the groups discussed. Because we are mainly interested in the hole-charge distribution over the different molecular units of the cluster, we have grouped together all contributions on atomic centers which are part of the same unit. In the outer-valence region (≈12−21 eV) the nine cationic states in Table 1a are mainly derived from 1h configuration contributions (main states). Because of this, the hole-population analysis of the sole 1h configuration space (1h-population analysis) already gives a good description of the charge distribution. Inclusion of the small 2h1p contributions changes the populations to some extent but does not affect the qualitative picture. Our main goal is to analyze the very many cationic states in the inner-valence region of the spectrum, so we shall not discuss the hole distribution of the outer-valence states in much detail. As expected, their nature can be qualitatively deduced already by inspection of the few dominating 1h eigenvector components, of F(2p) and O(2p) character. The hole distribution of the two lowest lying A″ states, for example, can be understood in terms of removing one electron from the two highest-lying occupied a″ orbitals, which are linear combinations of O(2p) orbitals having contributions on both H_2O units. The A″ state at about 15.18 eV has a fully localized hole on the HF unit, resulting from removal of one electron from the a″ orbital mainly localized on HF.

The situation in the inner-valence region (≈30−45 eV) is very different. Here, most cationic states have only minor 1h configuration contributions (satellite states with small spectral intensity) and are therefore mainly derived from excited cationic

TABLE 1: Spatial Hole-Charge Distribution of Selected Cationic States of the $HF(H_2O)_2$ Cluster Characteristic for the Different Energy Regions

	HF		$H_2O^{[1]}$		$H_2O^{[2]}$		$HF(H_2O)_2$		
IP[eV]	(1h)	(1h+2h1p)	(1h)	(1h+2h1p)	(1h)	(1h+2h1p)	(1h)	(1h+2h1p)	state
				(a) Outer-Valence States					
12.8384	0.0004	−0.0860	0.2876	0.2932	0.6252	0.7843	0.9132	0.9916	A″
13.2030	0.0137	−0.1276	0.6133	0.7868	0.2854	0.3321	0.9124	0.9913	A″
14.8031	0.1209	0.0674	0.3556	0.4098	0.4496	0.5130	0.9261	0.9903	A′
15.1051	0.7262	0.8314	0.1794	0.1639	0.0216	−0.0007	0.9272	0.9946	A′
15.1755	0.9044	1.0916	0.0098	−0.0612	0.0034	−0.0335	0.9176	0.9968	A″
15.6633	0.1963	0.1732	0.2937	0.3171	0.4364	0.5003	0.9265	0.9905	A′
18.5781	0.4054	0.4106	0.3932	0.4647	0.1282	0.1156	0.9268	0.9909	A′
19.1701	0.2358	0.2504	0.0711	−0.0111	0.6225	0.7506	0.9293	0.9899	A′
20.0221	0.1540	0.0826	0.5649	0.6907	0.2074	0.2164	0.9263	0.9897	A′
				(b) Inner-Valence States, O(2s) Decay Distribution					
35.0639	0.0001	0.3891	0.0076	0.2595	0.0004	0.3513	0.0082	1.0000	A′
35.0692	0.0000	0.4460	0.0037	0.1903	0.0017	0.3636	0.0054	1.0000	A′
35.1412	0.0001	0.4918	0.0259	0.2111	0.0029	0.2969	0.0289	0.9999	A′
35.1820	0.0001	0.2493	0.0144	0.4762	0.0005	0.2744	0.0151	0.9999	A′
35.5498	0.0000	0.3884	0.0087	0.0883	0.0008	0.5232	0.0094	1.0000	A′
35.5717	0.0001	0.4542	0.0104	0.4217	0.0001	0.1241	0.0106	0.9999	A′
35.5748	0.0002	0.2604	0.0465	0.4966	0.0012	0.2428	0.0478	0.9998	A′
35.5948	0.0002	0.4533	0.0090	0.3073	0.0035	0.2394	0.0127	0.9999	A′
				(c) Inner-Valence States, F(2s) Decay Distributions					
40.1089	0.0633	0.4936	0.0007	0.4898	0.0000	0.0165	0.0641	0.9999	A′
40.1120	0.0426	0.5406	0.0005	0.3299	0.0000	0.1294	0.0431	0.9999	A′
40.1234	0.0203	0.0200	0.0003	0.3402	0.0000	0.6398	0.0206	1.0000	A′
40.1255	0.0484	0.3929	0.0015	0.2285	0.0001	0.3785	0.0499	0.9999	A′
40.1763	0.0314	0.3501	0.0004	0.3172	0.0001	0.3327	0.0319	0.9999	A′
40.1834	0.0592	0.4390	0.0007	0.4235	0.0001	0.1356	0.0599	0.9999	A′
40.2025	0.0161	0.2994	0.0005	0.3781	0.0001	0.3224	0.0167	1.0000	A′
40.2129	0.0859	0.6604	0.0011	0.3924	0.0001	−0.0530	0.0871	0.9998	A′
				(d) Inner-Valence States, Outside Decay Distribution					
43.5043	0.0000	−0.0236	0.0015	0.8157	0.0000	0.2078	0.0015	0.9999	A″
43.6707	0.0000	0.0193	0.0000	−0.3001	0.0029	1.2808	0.0030	0.9999	A″
45.8188	0.0000	0.0909	0.0000	−0.1923	0.0029	1.1009	0.0030	0.9994	A′
47.7758	0.0000	0.1580	0.0000	−0.2784	0.0010	1.1203	0.0010	1.0000	A″
48.5580	0.0000	−0.3206	0.0000	−0.1280	0.0019	1.4484	0.0019	0.9999	A″
49.9207	0.0020	1.1502	0.0000	−0.1623	0.0000	0.0120	0.0020	0.9999	A′
50.5190	0.0014	1.4454	0.0000	−0.1830	0.0000	−0.2626	0.0015	1.0000	A″
50.6570	0.0026	0.8786	0.0000	−0.0796	0.0000	0.2010	0.0026	1.0000	A′

[a] Displayed are the ionization potentials (IPs) of the states together with the hole-populations on the different monomer units resulting from the hole-population analysis of the 1h and 1h+ 2h1p configuration contributions of the corresponding ADC(3) eigenvectors.

2h1p configurations in the ADC(3) scheme. In contrast to the spectral intensity in the photoionization spectrum, which is essentially related to the 1h components of the eigenvectors, the physical character of these satellite states can only be meaningfully described by taking the 2h1p contributions into consideration. Thus, the (1h+ 2h1p) population terms are the relevant quantities. Because we are mainly interested in analyzing the state distributions describing the electronic decay of inner-valence cationic states, we shall focus on the comparison between states inside such decay distributions and states that are not involved in decay bands.

The results of the hole-population analysis on the different types of inner-valence states are presented in Table 1b−d. Selected typical states involved in the O(2s) decay distribution between 34 and 36 eV are in Table 1b, and states involved in one of the two F(2s) decay distributions between 40 and 41 eV are in Table 1c, while selected states not involved in any decay distribution are in Table 1d. Inspection of the tiny 1h populations of the inner-valence states results in the general observation of a pronounced localization of the hole-charge on either the HF (F(2s) vacancies) or over the two H_2O units (O(2s) vacancies). Although this finding is of great importance for the understanding of the contributions to the spectral intensity in the photoionization process (sudden approximation) we have to look at the full (1h+2h1p) populations to gain a meaningful insight into the hole-charge distribution of the satellite states. This changes the picture drastically: In the decay distributions the net hole-charge of +1 is delocalized by comparable amounts on either two or all three monomer units, whereas the hole-charge remains mainly localized on only one molecule in the states not involved in the decay. This observation fits nicely with the proposed intermolecular character of the electronic decay of inner-valence vacancies.

The negative values which are observed in some of the (1h+2h1p) populations on the individual molecular units may be surprising at first sight but can be easily understood in terms of the character of the excited electron in the 2h1p configuration contributions. The 1p contributions can lead to the accumulation of negative charge in a specific spatial region despite the net positive charge of the cluster ion. Because of the more localized character of the hole density in states not involved in a decay distribution, an accumulation of negative charge is most likely in this kind of states (see Table 1d). The very small deviations of the total charge from unity are due to small couplings to anionic configurations, which arise because of the specific structure of the ADC eigenvalue problem (see section II). The anionic components are neglected in the hole-population analysis.

For reasons of simplicity we will focus in the further analysis mainly on the F(2s) decaying states. Here the situation is simpler

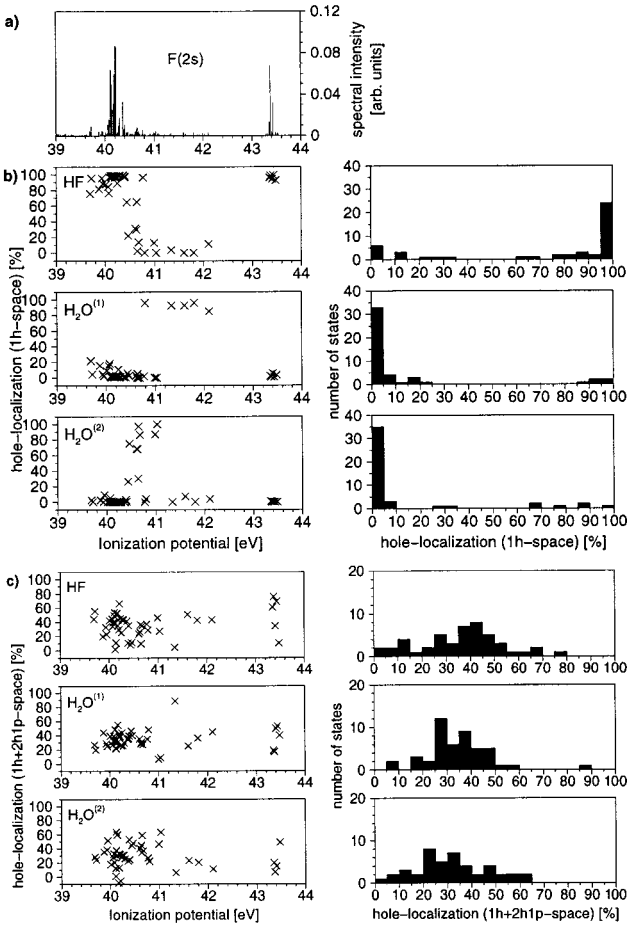

Figure 7. Spatial hole-charge distribution on the molecular units of the cluster for the states involved in the decay distributions of the two F(2s) inner-valence vacancies shown in (a). Plotted in the left-hand side graphs is the degree of localization of the hole-charge on the three molecular units: (b) considering only the 1h configuration space (1h population), (c) considering the full 1h+ 2h1p configuration space (1h+2h1p population). The corresponding histograms on the right-hand side show the number of states with a given degree of hole-localization.

compared to the O(2s) decay distributions because of several reasons. The weaker breakdown effects in the F(2s) spectral region lead to only two distinct decaying states, whereas in the O(2s) region configuration contributions are redistributed to a much larger extent over several lines, resulting in largely overlapping decay distributions. In addition, there is only one HF unit, resulting in a single molecular orbital with localized F(2s) character. The existence of two H_2O units, on the other hand, leads to two molecular orbitals with O(2s) character which are linear combinations of the two O(2s) atomic orbitals. Therefore, the 1h configuration contributions of the O(2s) vacancies are partially delocalized over the two H_2O units, whereas the localization of the F(2s) vacancies in 1h configuration space provides a simple starting point for the investigation of the decay mechanism after preparation of the vacancy in a sudden ionization process.

The states involved in the two F(2s) decay distributions are shown again, on an enlarged scale, in Figure 7 together with graphical representations of their degree of hole localization on the three molecular units, both in terms of 1h configurations only and of (1h+2h1p) configurations. If one considers only the 1h space contributions, practically all states in the two distributions are fully localized on the HF system (Figure 7b). As mentioned earlier, this picture characterizes the inner-valence states as localized F(2s) vacancies. In the full 1h+2h1p space,

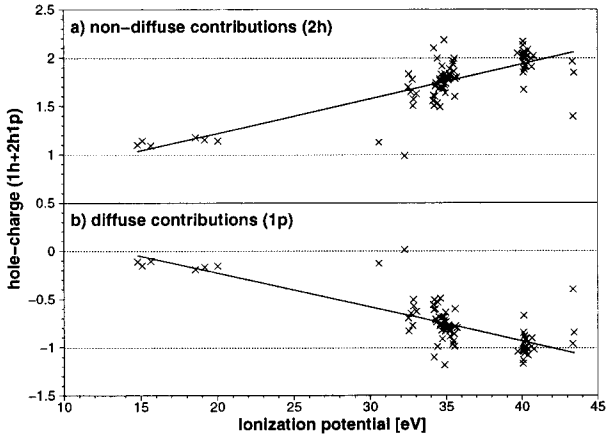

Figure 8. Partitioning of the net hole-charge in the cationic states with A′ symmetry into nondiffuse and diffuse basis set contributions. For the inner-valence, mainly 2h1p, states, the nondiffuse contributions approximate the 2h part and the diffuse contributions approximate the 1p part. The dotted lines represent the ideal values of + 1 (1h) and 0 for the outer-valence and of +2 (2h) and −1 (1p) for the inner-valence. The solid lines are cubic fits to the individual partitioned hole-charge distributions.

these vacancies decay electronically via coupling to the continuum of dicationic states mimicked by the 2h1p configurations. In Figure 7c the hole distribution in the full configuration space is displayed, showing indeed that in reality all states in the decay distributions have a hole density largely delocalized on two or on all three molecular units, thus demonstrating the intermolecular character of the decay process.

To arrive at a more illustrative picture of the hole-charge pattern in the satellite states of the inner-valence region, we have partitioned the atomic orbital contributions to the hole-populations into two further subgroups (see section III) comprising basis functions of nondiffuse character (cc-pVDZ basis functions) and the diffuse basis functions, respectively. For the clusters of satellite 2h1p states, one should thereby expect that the nondiffuse component describes essentially the two-hole part of the charge density, while the diffuse contribution describes the particle (excited, or escaping, electron). This deconvolution works nicely, as can be seen in Figure 8, where the two computed components just described are plotted in separate graphs for each of the states of A′ symmetry. In the low-energy outer-valence region the whole charge is essentially described entirely by the nondiffuse contributions (of 1h type). Proceeding toward the inner-valence region, where the 2h1p character dominates, the nondiffuse and diffuse contributions progressively approach the ideal values of +2 (2h) and −1 (1p), respectively.

The nondiffuse and diffuse contributions to the hole-charge distribution on the different monomer units are shown in Figure 9a for the whole inner-valence area. From this deconvolution we are now able to extract direct information on the distribution of the two holes and the excited electron over the different units in the satellite states. Upon comparing states inside a decay distribution with nondecaying states, a major difference is observed in the nondiffuse contributions: In the decay bundles the two holes are distributed over two or, in most cases, over all three molecular units, whereas they are to a very large extent localized on only one unit in the states lying outside the decay bands. The differences in the spatial distribution of the excited electron are not so obvious for the different kind of states because of the diffuse character of the basis functions. Nevertheless, trends can be observed, in that the excited electron in a state belonging to a decay distribution is roughly equally

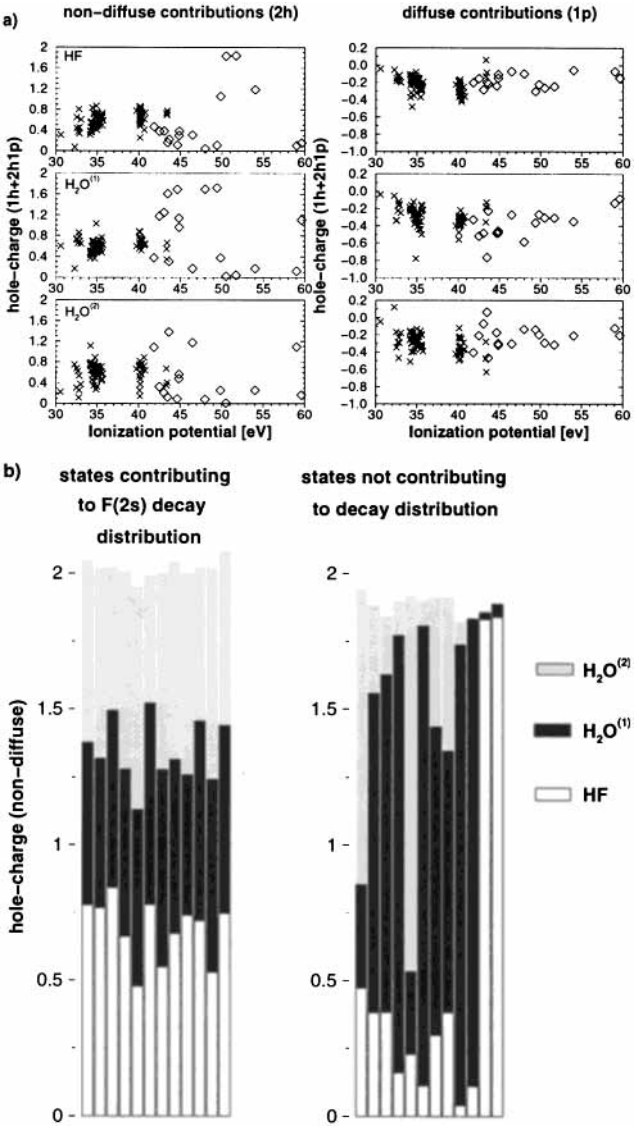

Figure 9. (a) Spatial hole-charge distribution on the different molecular units of the cluster decomposed into nondiffuse (2*h*) and diffuse (1*p*) contributions, for the inner-valence ionized states. States involved in decay distributions are labeled ×, states outside decay distributions are labeled ◇. (b) Hole-charge composition of selected individual states in the F(2s) decay band between 40 and 41 eV (left part) and of states not involved in any decay distribution (right part). Clearly evidenced is the contrast between the hole delocalization over all three molecular units in the decay states and the pronounced hole localization at only one molecular site of the nondecaying states.

distributed over the whole system, while in a nondecaying state it tends to be somewhat more localized on the monomer unit where the two holes are localized. In Figure 9b the charge distribution of the two holes (i.e., the nondiffuse component of the population) is compared for selected individual states inside one of the F(2s) decay distributions and states not involved in the decay. The uniform delocalization of the two holes in the states representing the electronic decay is in sharp contrast with the distinct localization of the two holes on one molecular unit for the nondecaying states.

We summarize the emerging picture of the decay of a F(2s) vacancy. The situation is similar in the case of the other vacancies. The decaying inner-valence F(2s) vacancy, produced by ionization of the neutral ground state system, is localized on the HF unit. This has been confirmed by analyzing the hole-charge distribution of the vacancy in the 1h configuration space. Only this space contributes to the spectral intensity (sudden approximation). In the ADC(3) Green's function calculations, the electronic decay of the prepared F(2s) vacancy leading to dicationic states is described via coupling of the 1h configurations of the vacancy to excited 2h1p configurations. These 2h1p configurations represent the coupling of the cationic state to the continua of the accessible dicationic decay channels in our discrete finite basis set approach. The coupling is visible in the spectrum as dense line bundles of satellite states grouped around the decaying state. In a simple picture, the 2h part of the 2h1p configurations mimics the 2h configurations of the evolving dicationic decay channels, the 1p part mimics the corresponding outgoing electron. Although the two vacancies (2h configuration contributions) of the individual dicationic decay channels are localized mainly on only two neighboring molecular units (see section IVc), the 2h components of the cationic states representing the decay distributions are typically delocalized over all three units. This finding can be understood in a simple way in terms of the strong configuration mixing responsible for the coupling to all possible dicationic decay channels: The uniformly delocalized charge distribution of the cationic states reflects an average of the charge distribution over all the dicationic states available to the decay.

E. Decaying State Lifetimes. To demonstrate the efficiency of the proposed ICD mechanism, we have estimated the lifetimes of the inner-valence vacancies F(2s) vacancies. For this purpose, the results of the largest performed calculation on the ionization spectrum of $HF(H_2O)_2$ (aug-cc-pVDZ basis set) have been used exclusively.

As mentioned earlier, in a discrete basis set representation the inherent energy broadening of the decaying states in the ionization spectrum is mimicked by dense line bundles. For IP $<$ 45 eV, all individual lines in this computed stick spectrum correspond to accurately converged eigenvectors. As already done in ref 18, we can better simulate the line broadening of the decaying states by convoluting the discrete lines in the bundles by Gaussian functions of fixed full-width at half-maximum (fwhm). The resulting spectral envelope is then least-squares fitted by a single Lorentzian function. The fwhm of this fitted Lorentzian provides a measure of the decay width and therefore of the lifetime of the decaying inner-valence vacancy. Because of the several open dicationic decay channels contributing to the decay width (see Figure 5), which is now represented by a single Lorentzian distribution, the estimated lifetime is a measure of the sum of the individual decay-channel contributions. The accuracy of the estimated lifetime can be improved by repeating the above procedure using successively smaller fwhms of the Gaussian functions with which the single lines are convoluted.

We have restricted the lifetime estimate to the F(2s) vacancies in the $HF(H_2O)_2$ cluster because of the much simpler situation compared to the O(2s) vacancies (see discussion in section IVD). The convoluted stick spectra for the two F(2s) decay distributions at about 38.3 and 41.7 eV are shown in Figure 10, together with the Lorentzian curves that best fit the spectral envelope in a least-squares sense. The widths of the Lorentzian distributions are computed to be 0.08 eV (distribution at lower IP) and 0.07 eV (distribution at higher IP) corresponding to lifetimes of 8.2 and 9.4 fs, respectively. These values are very close to those obtained in a similar manner for the $(HF)_3$ cluster in a study on the inner-valence vacancies of small $(HF)_n$ clusters.[18] We note that these values are comparable in magnitude to the lifetime of the F(1s) core hole which decays by the usual (intra-atomic) Auger mechanism. The F(1s) core hole has a decay width of

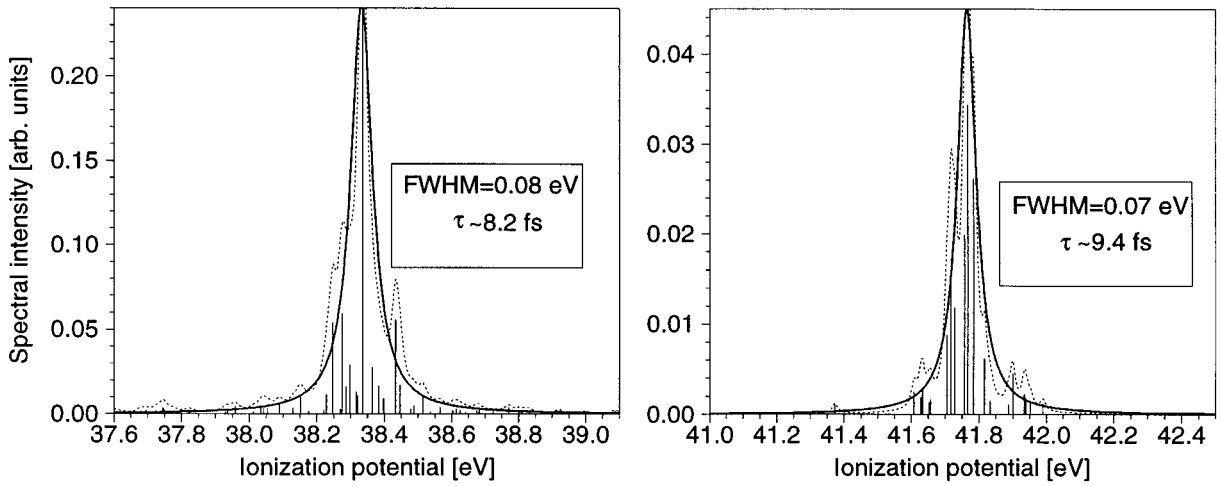

Figure 10. Estimate of the decay widths (lifetimes) of the two F(2s) inner-valence vacancies of the $HF(H_2O)_2$ cluster. The computed discrete lines representing the decay channels of a cationic state (stick spectrum) are convoluted by Gaussian functions of fwhm 0.02 eV. The resulting spectral envelope (dotted line) is least-squares fitted with a Lorentzian function describing the resonance energy profile (solid line). The resonance parameters (width and lifetime τ) resulting from the fitted Lorentzian curves are shown.

about 0.2 eV, corresponding to a lifetime of about 3.3 fs.[44] This lifetime is characteristic of the fluorine atom and depends only marginally on the environment of the atom, in sharp contrast to the ICD of the F(2s) vacancy studied here which actually is a phenomenon taking place only in the presence of an environment.

It should be clear from the described procedure that the estimated lifetimes cannot be considered to be highly accurate, for several reasons. The resonances decay by electron correlation and their lifetimes are difficult to compute. Apart from the fact that we use a discrete finite basis set for the calculation of resonances there are additional restrictions in the method itself. Because of the large-scale eigenvalue problem there is only limited capability in using extended basis sets and also in performing extensive basis set studies. In the description of the satellite states only 2h1p configurations are considered as excited configurations in the ADC(3) approach. In a recent study on the inner-valence vacancies of the $(HF)_2$ cluster[19] using a standard CI method augmented by a complex absorbing potential (CAP) the resonance parameters have been calculated in a more quantitative way. By the CAP−CI method the energy of the resonance is continued into the complex energy plane. In this way one avoids to estimate the lifetime from a discrete stick spectrum. The first results obtained with this CAP−CI method on the $(HF)_3$ cluster[45] nicely confirm the values estimated in a recent study[18] on the same system with the method presented here.

5. Conclusions and Outlook

In the present work we have investigated in detail the electronic decay of singly ionized inner-valence states of molecular clusters in an exemplary study on the cyclic $HF(H_2O)_2$ cluster. We have shown that, in sharp contrast to the constituent isolated monomer molecules, the inner-valence vacancies in the molecular cluster can efficiently decay via the intermolecular Coulombic decay (ICD) mechanism which has been proposed recently in studies on singly and doubly ionized inner-valence states of small $(HF)_n$ and $(H_2O)_n$ clusters.[17,18]

The decay effects have been analyzed by calculating the ionization spectra of the clusters using large scale ab initio Green's function methods. In our finite discrete basis set calculations (L^2-approach), the broadened bands which should appear in the ionization spectrum corresponding to transitions from the neutral ground state to electronically decaying cationic states are mimicked by dense bundles of lines grouped around the positions of the decaying states in a characteristic way. By analyzing these line bundles, the lifetimes of the inner-valence vacancies have been estimated to be of the order of few femtoseconds, being comparable to the lifetimes of atomic core vacancies due to Auger decay.

The proposed ICD mechanism can be summarized as follows: an outer-valence electron of the molecular site carrying the initial inner-valence vacancy drops into this vacancy and the resulting excess energy is transferred in an ultrafast process to a neighboring monomer unit, where it causes the ejection of an outer-valence electron. The decay process, therefore, leads to outer-valence dicationic states having the two vacancies distributed over neighboring molecular units. Subsequent fragmentation of the weakly bound molecular cluster because of the Coulomb repulsion of the positive charges is likely.

By evaluating the accessible outer-valence dicationic decay channels for the cationic inner-valence vacancies, we were able to show that, because of energetic reasons, only an intermolecular decay mechanism is possible in the molecular clusters. In these systems, a substantial lowering of the energy onset of the dicationic states is observed, compared to the isolated constituent molecules, due to the possible localization of the two vacancies on different monomer units, with consequently reduced hole−hole repulsion. In this way, autoionization decay channels are open in the cluster ions which are not available in the isolated constituent molecules. The observed high efficiency of the decay can be understood in terms of the large number of accessible decay channels resulting from the many possible ways to distribute the two vacancies in the clusters, in combination with the nonnegligible Coulombic matrix elements responsible for the efficient energy transfer between the neighboring monomer units.[17,18]

The intermolecular character of the observed decay process of inner-valence vacancies has been confirmed in a direct way by a careful investigation of the line bundles representing the broadened decaying states in the calculated ionization spectra. This task has been accomplished by devising a method of analysis of the hole-density in the ionized states. In this hole-population analysis the charge density of each calculated cationic

state is partitioned into contributions spatially localized on the different molecular units of the cluster. We have thus been able to show that all the states contributing to the decay distributions are intermolecular in character, in that the hole-charge density is distributed over neighboring monomer units. It should be noted that, beyond its diagnostic value in the investigation of the decay mechanism, the hole-population analysis provides a powerful tool for the characterization and understanding of the nature of the very many ionized states typical of the inner-valence region of many molecular systems in general.

To confirm experimentally the proposed ICD effect by inspection of the ionization spectra may not be easy because of the limited experimental resolution and other effects such as vibrational broadening. We therefore propose a more direct way to study the decay effects experimentally. After preparation of the, possibly size-selected, singly ionized clusters in a molecular beam apparatus using synchrotron radiation, above a specific threshold energy a second electron due to the electronic decay should be detected in coincidence with the primary photoelectron. In a comparative experiment on the isolated molecules that build up the clusters no secondary electron should be observed in the inner-valence energy region. Additional hints of the intermolecular character of the decay could be obtained by detection of specific ionic fragmentation products resulting from Coulomb repulsion of the dicationic decay products having charges localized on neighboring monomer units. It should of course be considered that the appearance of fragmentation products can, at least in principle, result from the same dicationic states produced by direct double photoionization (see, e.g., ref 46). However, direct double photoionization, as a one-photon-two-electron interaction process, is much more inefficient in the production of dicationic states, especially in the case that these states are intermolecular in nature, compared to their production via ICD of the singly ionized inner-valence vacancies. The additional possibility should also be considered that the final dicationic states are produced by secondary ionization caused by the collision of the primary photoelectron with a neighboring monomer unit,[47,48] a situation not included in our ab initio calculations. This event can, however, be easily distinguished from the ICD mechanism because of the very different kinetic energy distribution of the primary photoelectron.

To extend the knowledge of the decay processes studied here, further investigations in two principal directions seem to be appropriate. The ICD mechanism prevails in singly and doubly ionized inner-valence states of molecular clusters, but it is of more general nature and we expect it to be active in neutral electronically excited states and all types of weakly bound systems as well. This includes, e.g., molecules adsorbed on surface layers. The Green's function methods used so far have turned out to be very useful, but are not suited to give a highly accurate description of the decay effects because of the limitations imposed by the discrete finite basis sets. For the more quantitative determination of the resonance parameters (energy, lifetime) of the decaying states these methods have to be extended by taking into consideration in a more systematic way the continuum character of the outgoing electron. Guidelines for these extensions have already been given by augmenting standard quantum chemical methods with complex absorbing potentials in the study of the resonances of small molecular clusters.[19]

Acknowledgment. Financial support by the Deutsche Forschungsgemeinschaft (DFG) is gratefully acknowledged.

Appendix A: Spin-Free Working Equations for the Hole-Density Analysis of the Cationic States

In the $M_s = {}^1/_2$ space and summing over spatial orbitals, the (assumed normalized) nth cationic state wave function in 1h and 2h1p configuration space reads

$$|\Psi_n^{N-1}\rangle = \sum_i A_i|\Phi_i\rangle + \sum_{r,i} A_{rii}|\Phi_{rii}\rangle + \sum_{r,i>j}\{A'_{rij}|\Phi'_{rij}\rangle + A''_{rij}|\Phi''_{rij}\rangle\} \quad \text{(A1)}$$

where the spin eigenfunctions used are

$$|\Phi_i\rangle = a_{\bar{i}}|\Phi_0\rangle \equiv |\Phi_{\bar{i}}\rangle$$

$$|\Phi_{rii}\rangle = a_r^\dagger a_i a_{\bar{i}}|\Phi_0\rangle \equiv |\Phi_{r\bar{i}i}\rangle$$

$$|\Phi'_{rij}\rangle = \frac{1}{\sqrt{2}}(a_r^\dagger a_i a_{\bar{j}} - a_r^\dagger a_{\bar{i}} a_j)\,|\Phi_0\rangle \equiv \frac{1}{\sqrt{2}}(|\Phi_{r\bar{i}j}\rangle - |\Phi_{r\bar{i}\bar{j}}\rangle) \quad \text{(A2)}$$

$$|\Phi''_{rij}\rangle = -\frac{1}{\sqrt{6}}(2a_{\bar{r}}^\dagger a_{\bar{i}} a_{\bar{j}} + a_r^\dagger a_i a_{\bar{j}} + a_r^\dagger a_{\bar{i}} a_j)|\Phi_0\rangle \equiv -\frac{1}{\sqrt{6}}(2|\Phi_{\bar{r}\bar{i}\bar{j}}\rangle + |\Phi_{r\bar{i}j}\rangle + |\Phi_{r\bar{i}\bar{j}}\rangle)$$

and the bar (absence thereof) over the orbitals denotes spin β-(α). Thus we can rewrite

$$|\Psi_n^{N-1}\rangle = \sum_i A_i|\Phi_{\bar{i}}\rangle + \sum_{r,i} A_{rii}|\Phi_{r\bar{i}\bar{i}}\rangle + \sum_{r,i>j}\{B_{rij}|\Phi_{\bar{r}\bar{i}\bar{j}}\rangle + C_{rij}|\Phi_{r\bar{i}j}\rangle + D_{rij}|\Phi_{r\bar{i}\bar{j}}\rangle\} \quad \text{(A3)}$$

where

$$B_{rij} = -\frac{2}{\sqrt{6}}A''_{rij}$$

$$C_{rij} = -\left(\frac{A''_{rij}}{\sqrt{6}} - \frac{A'_{rij}}{\sqrt{2}}\right) \quad \text{(A4)}$$

$$D_{rij} = -\left(\frac{A''_{rij}}{\sqrt{6}} + \frac{A'_{rij}}{\sqrt{2}}\right)$$

Rewriting the 1h and 2h1p terms of eq 5 of section III in terms of spatial orbitals, by comparison with eq A3, we now establish that the following coefficients are nonzero:

$$x_{\bar{i}} = A_i$$

$$x_{r\bar{i}\bar{j}} = \begin{cases} C_{rij} & \text{for } i > j \\ A_{rii} & \text{for } i = j \end{cases}$$

$$x_{r\bar{i}j} = \begin{cases} D_{rij} & \text{for } i > j \\ -A_{rii} & \text{for } i = j \end{cases} \quad \text{(A5)}$$

$$x_{\bar{r}\bar{i}\bar{j}} = B_{rij}$$

This allows us to explicity separate spins in eq 7 of section III obtaining, for the α hole-density,

$$\Delta_{ij}(i>j) = \sum_{r,k} x^*_{r[j\bar{k}]} x_{r[i\bar{k}]}$$
$$= \sum_r \{ \sum_{\substack{k \\ (k<j)}} C^*_{rjk} C_{rik} - \sum_{\substack{k \\ (i>k>j)}} D^*_{rkj} C_{rik} + \sum_{\substack{k \\ (k>i)}} D^*_{rkj} D_{rki} - D^*_{rij} A_{rii} + A^*_{rjj} C_{rij} \}$$

$$\Delta_{ii} = \sum_{r,k} |x_{r[i\bar{k}]}|^2$$
$$= \sum_r \{ \sum_{\substack{k \\ (k<i)}} |C_{rik}|^2 + \sum_{\substack{k \\ (k>i)}} |D_{rki}|^2 + |A_{rii}|^2 \}$$

$$\Delta_{ri} = -\sum_j x^*_{r[\bar{ij}]} x_{\bar{j}} \qquad \text{(A6)}$$
$$= -\sum_{\substack{j \\ (j<i)}} C^*_{rij} A_j + \sum_{\substack{j \\ (j>i)}} D^*_{rji} A_j - A^*_{rii} A_i$$

$$\Delta_{rs}(r \geq s) = -\sum_{i>j} \{ x^*_{ri\bar{j}} x_{si\bar{j}} + x^*_{ri\bar{j}} x_{sij} \} - \sum_i x^*_{ri\bar{i}} x_{si\bar{i}}$$
$$= -\sum_{i>j} \{ C^*_{rij} C_{sij} + D^*_{rij} D_{sij} \} - \sum_i A^*_{rii} A_{sii}$$

while the β hole-density becomes

$$\Delta_{\bar{i}\bar{j}}(i>j) = x^*_{\bar{j}} x_{\bar{i}} + \sum_{\substack{r,k \\ (k\neq i,j)}} \{ x^*_{r[\bar{j}k]} x_{r[\bar{i}k]} + x^*_{\bar{r}[jk]} x_{\bar{r}[ik]} \} + \sum_r \{ x^*_{r[\bar{j}i]} x_{r[\bar{i}i]} + x^*_{r[\bar{j}j]} x_{r[\bar{i}j]} \}$$
$$= A^*_j A_i + \sum_r \{ \sum_{\substack{k \\ (k<j)}} D^*_{rjk} D_{rik} - \sum_{\substack{k \\ (i>k>j)}} C^*_{rkj} D_{rik} + \sum_{\substack{k \\ (k>i)}} C^*_{rkj} C_{rki} + \sum_k B^*_{r[jk]} B_{r[ik]} + C^*_{rij} A_{rii} - A^*_{rjj} D_{rij} \} \qquad \text{(A7)}$$

$$\Delta_{ii} = |x_{\bar{i}}|^2 + \sum_{\substack{r,k \\ (k\neq i)}} \{ |x_{r[\bar{i}k]}|^2 + |x_{\bar{r}[ik]}|^2 \} + \sum_r |x_{r[\bar{i}i]}|^2$$
$$= |A_i|^2 + \sum_r \{ \sum_{\substack{k \\ (k<i)}} |D_{rik}|^2 + \sum_{\substack{k \\ (k>i)}} |C_{rki}|^2 + \sum_k |B_{r[ik]}|^2 + |A_{rii}|^2 \}$$

$$\Delta_{r\bar{i}} = -\sum_j x^*_{r[ij]} x_{\bar{j}} = -B^*_{r[ij]} A_j$$

$$\Delta_{r\bar{s}} = -\sum_{i>j} x^*_{rij} x_{\bar{sij}} = -\sum_{i>j} B^*_{rij} B_{sij}$$

The spinless hole-density is obtained by summing the α and β components. By further defining

$$A'_{r\{ij\}} = \begin{cases} A'_{rij} & \text{for } i>j \\ 0 & \text{for } i=j \\ A'_{rji} & \text{for } i<j \end{cases} \qquad \text{(A8)}$$

the final result for the spinless hole-density matrix elements reads

$$\Delta_{ij}(i>j) = A^*_j A_i + \sum_{r,k} \{ A'^*_{r\{jk\}} A'_{r\{ik\}} + A'^*_{r[jk]} A''_{r[ik]} \} + \sqrt{2} \sum_r \{ A'^*_{rij} A_{rii} + A^*_{rjj} A'_{rij} \}$$

$$\Delta_{ii} = |A_i|^2 + \sum_{r,k} \{ |A'_{r\{ik\}}|^2 + |A''_{r[ik]}|^2 \} + 2 \sum_r |A_{rii}|^2$$

$$\Delta_{ri} = -A^*_{rii} A_i - \frac{1}{\sqrt{2}} \sum_j (A'^*_{r\{ij\}} - \sqrt{3} A''^*_{r[ij]}) A_j$$

$$\Delta_{rs} = -\sum_{i>j} \{ A'^*_{rij} A'_{sij} + A''^*_{rij} A''_{sij} \} - \sum_i A^*_{rii} A_{sii}$$

References and Notes

(1) *Science* **1996**, *271*, 920 (special issue on clusters).
(2) *Clusters of Atoms and Molecules I*; Haberland, H., Ed.; Springer Series in Chemical Physics 52; Springer: Berlin, 1994, and references therein.
(3) *Chem. Rev.* **1988**, *88*, 813 (*van der Waals Molecules*).
(4) *Chem. Rev.* **1994**, *94*, 1721 (*van der Waals Molecules II*).
(5) Hobza, P.; Zahradnik, R. *Intermolecular Complexes*; Elsevier: Amsterdam, 1988.
(6) Müller-Dethlefs, K.; Dopfer, O.; Wright, T. G. *Chem. Rev.* **1994**, *94*, 1845, and references therein.
(7) Rühl, E.; Knop, A.; Hitchcock, A. P.; Dowben, P. A.; McIlroy, D. N. *Surf. Rev. Lett.* **1996**, *3*, 557.
(8) Federmann, F.; Björneholm, O.; Beutler, A.; Möller, T. *Phys. Rev. Lett*. **1994**, *73*, 1549.
(9) Björneholm, O.; Federmann, F.; Fössing, f.; Möller, T. *Phys. Rev. Lett.* **1995**, *74*, 3017.
(10) Eland, J. H. D. *Photoelectron Spectroscopy*, 2nd ed.; Butterworth: 1984.
(11) Turner, D. W.; Baker, C.; Baker, A. D.; Brundle, C. R. *Molecular Photoelectron Spectroscopy*; Wiley: New York, 1970.
(12) Öhrwall, G.; Sundin, S.; Baltzer, G.; Bozek, J. *J. Phys. B: At. Mol. Phys.* **1999**, *32*, 463.
(13) Yencha, A. J.; McConkey, A. G.; Dawber, G.; Avaldi, L.; MacDonald, M. A.; King, G. C.; Hall, R. I. *J. Electron Spectrosc. Relat. Phenom*. **1995**, *73*, 217
(14) Yencha, A. J.; Cormack, A. J.; Donovan, R. J.; Hopkirk, A.; King, G. C. *Chem. Phys.* **1998**, *238*, 109.
(15) Azaroff, L. V. *X-ray Spectroscopy*; McGraw-Hill: New York, 1974.
(16) Thompson, M.; Baker, M. D.; Christie, A.; Tyson, J. F. *Auger Electron Spectroscopy*; Wiley: New York, 1985.
(17) Cederbaum, L. S.; Zobeley, J.; Tarantelli, F. *Phys. Rev. Lett.* **1997**, *79*, 4778.
(18) Zobeley, J.; Cederbaum, L. S.; Tarantelli, F. *J. Chem. Phys.* **1998**, *108*, 9737.
(19) Santra, R.; Cederbaum, L. S.; Meyer, H.-D. *Chem. Phys. Lett.* **1999**, *303*, 413.
(20) Schirmer, J.; Cederbaum, L. S.; Walter, O. *Phys. Rev. A* **1983**, *28*, 1237.
(21) Tarantelli, A.; Cederbaum, L. S. *Phys. Rev. A* **1989**, *39*, 1639.
(22) Tarantelli, A.; Cederbaum, L. S. *Phys. Rev. A* **1989**, *39*, 1656.
(23) Schirmer, J. *Phys. Rev. A* **1991**, *43*, 4647.
(24) von Niessen, W.; Schirmer, J.; Cederbaum, L. S. *Comput. Phys. Rep.* **1984**, *1*, 57.
(25) Weikert, H.-G.; Meyer, H.-D.; Cederbaum, L. S.; Tarantelli, F. *J. Chem. Phys.* **1996**, *104*, 7122.
(26) Mattuck, A. D. *A Guide to Feynman Diagrams in the Many-Body Problem*; McGraw-Hill: New York, 1967.
(27) Cederbaum, L. S. In *The Encyclopedia of Computational Chemistry*, Schleyer, P. v. R., Allinger, N. L., Clark, T., Gasteiger, J., Kollman, P. A., Schaefer, H. F., III; Schreiner, P. R., Eds.; Wiley: Chichester, 1998.
(28) Golod, A.; Deleuze, M. S.; Cederbaum, L. S. *J. Chem. Phys.* **1999**, *110*, 6014.
(29) Meyer, H.-D.; Pal, S. *J. Chem. Phys.* **1989**, *91*, 6195.
(30) Schirmer, J.; Barth, A. *Z. Phys. A* **1984**, *317*, 267.
(31) Gottfried, F. O.; Cederbaum, L. S.; Tarantelli, F. *Phys. Rev. A* **1996**, *53*, 2118.
(32) Tarantelli, F. To be published.
(33) Tarantelli, F.; Sgamellotti, A.; Cederbaum, L. S. *J. Chem. Phys.* **1991**, *94*, 523.

(34) Rovira, C.; Constans, P.; Whangbo, M.-H.; Novoa, J. J. *Int. J. Quantum Chem.* **1994**, *52*, 177.
(35) Guest, M. F.; Kendrick, J.; van Lenthe, J. H.; Schoeffel, K.; Sherwood, P. *GAMESS−UK User's Guide and Reference Manual*; Computing for Science: Daresbury Laboratory, 1996.
(36) Dunning, T. H., Jr. *J. Chem. Phys.* **1989**, *90*, 1007.
(37) Cederbaum, L. S.; Domcke, W.; Schirmer, J.; von Niessen, W. *Adv. Chem. Phys.* **1986**, *65*, 115.
(38) Novoa, J. J.; Planas, M.; Whangbo, M.-H.; Williams, J. M. *Chem. Phys.* **1994**, *186*, 175.
(39) Hannachi, Y.; Silvi, B.; Bouteiller, Y. *J. Chem. Phys.* **1992**, *97*, 1911.
(40) Andrews, L.; Johnson, G. L. *J. Chem. Phys.* **1983**, *79*, 3670.
(41) Liegener, C.-M.; Chen, R. *J. Chem. Phys.* **1988**, *88*, 2618.
(42) Ramaker, D. E. *Chem. Phys.* **1983**, *80*, 183.
(43) von Niessen, W.; Cederbaum, L. S.; Domcke, W.; Diercksen, G. H. F. *Chem. Phys.* **1981**, *56*, 43.
(44) Uda, M.; Maeda, K.; Kayoma, A.; Sasa, Y. *Phys. Rev. A* **1984**, *29*, 1258
(45) Santra, R.; Cederbaum, L. S.; Meyer, H.-D. Unpublished results.
(46) Dujardin, G.; Leach, S.; Dutuit, O.; Guyon, P.-M.; Richard-Viard, M. *Chem. Phys.* **1984**, *88*, 339.
(47) Rühl, E.; Schmale, C.; Schmelz, H. C.; Baumgärtel, H. *Chem. Phys. Lett.* **1992**, *191*, 430.
(48) Biester, H. W.; Besnard, M. J.; Dujardin, G.; Hellner, L.; Koch, E. E. *Phys. Rev. Lett.* **1987**, *59*, 1277.